

SemCovNet: Towards Fair and Semantic Coverage-Aware Learning for Underrepresented Visual Concepts

Sakib Ahammed, Xia Cui, Xinqi Fan, Wenqi Lu, and Moi Hoon Yap

Department of Computing and Mathematics, Manchester Metropolitan University
The Dalton Building, Chester Street, M1 5GD Manchester

SAKIB.AHAMMED@stu.mmu.ac.uk and {X.Cui, X.Fan, W.Lu, M.Yap}@mmu.ac.uk

Abstract

Modern vision models increasingly rely on rich semantic representations that extend beyond class labels to include descriptive concepts and contextual attributes. However, existing datasets exhibit Semantic Coverage Imbalance (SCI), a previously overlooked bias arising from the long-tailed semantic representations. Unlike class imbalance, SCI occurs at the semantic level, affecting how models learn and reason about rare yet meaningful semantics. To mitigate SCI, we propose Semantic Coverage-Aware Network (SemCovNet), a novel model that explicitly learns to correct semantic coverage disparities. SemCovNet integrates a Semantic Descriptor Map (SDM) for learning semantic representations, a Descriptor Attention Modulation (DAM) module that dynamically weights visual and concept features, and a Descriptor–Visual Alignment (DVA) loss that aligns visual features with descriptor semantics. We quantify semantic fairness using a Coverage Disparity Index (CDI), which measures the alignment between coverage and error. Extensive experiments across multiple datasets demonstrate that SemCovNet enhances model reliability and substantially reduces CDI, achieving fairer and more equitable performance. This work establishes SCI as a measurable and correctable bias, providing a foundation for advancing semantic fairness and interpretable vision learning. Code will be released upon acceptance.

1. Introduction

Deep neural networks have achieved remarkable success across vision tasks—from object and scene recognition to fine-grained and medical image analysis [36, 69]. However, despite high overall accuracy, models often exhibit uneven performance across subgroups (e.g., appearance, context, or demographic attributes) and fail to recognize underrepresented visual concepts [60]. Existing fairness and debiasing strategies mainly address class imbalance or demographic

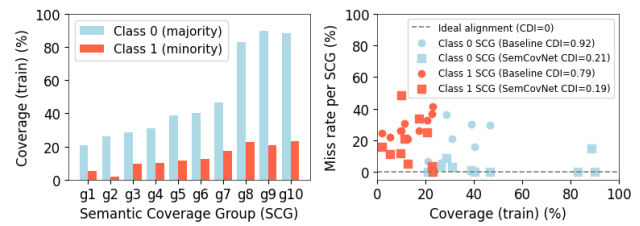


Figure 1. Semantic Coverage Imbalance. (Left) Long-tailed distribution of training coverage across Semantic Coverage Groups (SCGs) $g = (\text{class}, \text{descriptor}, \text{subgroup})$; minority SCGs consistently show lower coverage, indicating substantial semantic representation imbalance. (Right) Coverage–performance alignment across SCGs; greater deviation from ideal alignment indicates stronger coverage–error misalignment, motivating coverage-aware fairness learning. SemCovNet achieves lower Coverage Disparity Index (CDI), demonstrating improved semantic fairness.

bias, overlooking disparities within the semantic structure of the data [50]. We define this phenomenon as *Semantic Coverage Imbalance* (SCI)—the unequal representation of semantic descriptors (e.g., attributes, visual traits, or diagnostic cues) within and across classes (Fig. 1). For example, medical images are fundamentally semantic in nature. Each lesion is characterized by interpretable descriptors—visual attributes such as blue-white veil, streaks, or irregular pigment network [3, 6]. However, the training data exhibits an imbalance in descriptor representation, with some appearing frequently and others occurring in only a limited number of samples [48]. Unlike class imbalance, SCI arises at the visual concept-level, leading to biased feature learning, poor generalization to rare semantics, and unstable model interpretability. As a result, even a well-calibrated classifier may fail on under-covered descriptors, creating hidden sources of unfairness and reduced reliability in model predictions.

In recent years, fairness-aware learning has gained increasing attention in computer vision, particularly under long-tailed and imbalanced data distributions. Recent ad-

vances in balanced feature learning [2, 63], subgroup bias mitigation [67], and invariant representation approaches [7, 28, 39] aim to ensure equitable performance across imbalanced classes or latent environments. In medical imaging, recent studies highlight persistent subgroup and demographic disparities despite improved accuracy [32, 38]. These advances primarily address subgroup-level fairness, i.e., reducing worst-subgroup error or improving domain robustness. However, they remain agnostic to the semantic composition of visual concepts. Therefore, bias arising from unequal semantic representation within classes remains overlooked. Furthermore, beyond demographic or class-level imbalance, fine-grained visual understanding requires fairness at the semantic level—ensuring balanced learning across interpretable attributes and descriptors that define visual concepts. Real-world datasets contain latent and co-occurring semantic factors whose frequencies are highly skewed, forming hidden long tails that distort attention and feature alignment [12, 13, 50, 68]. Therefore, addressing SCI requires a reasoning process that is semantically aware, coverage-balanced, and interpretable.

Despite its significance, SCI has received little attention in vision research. Prior fairness and calibration studies typically measure outcomes only at the class level [55, 59], whereas concept-bottleneck models utilize descriptors as interpretable labels [56, 64], rather than focusing on coverage disparity. No existing framework explicitly models SCI during training, adapts attention to semantic rarity, and evaluates semantic fairness. To address these gaps, we propose SemCovNet that integrates descriptor semantics directly into visual representation learning. SemCovNet employs a Semantic Descriptor Map (SDM) and Descriptor Attention Modulation (DAM) to align visual features with underrepresented descriptors adaptively. A Coverage Disparity Index (CDI) regularizer minimizes the correlation between descriptor coverage and model error, ensuring semantic fairness through coverage–performance alignment.

Our main contributions are summarized as follows:

- We introduce the concept of Semantic Coverage Imbalance (SCI) as a fundamental and overlooked source of unfairness in visual concepts, highlighting how uneven descriptor representation skews learning and reasoning.
- We propose SemCovNet, a Semantic Coverage-Aware framework that integrates descriptor–visual concepts through SDM, DAM, and Descriptor–Visual Alignment (DVA), enabling semantically interpretable, and generalizable representations for rare or uncertain descriptors.
- We use CDI as both a metric and a regularizer to quantify SCI and reduce coverage–error misalignment for semantic fairness.
- Extensive experiments demonstrate that SemCovNet consistently reduces CDI while improving reliability and calibration, achieving fairer and more interpretable recogni-

tion across diverse datasets.

2. Related Work

Class imbalance and long-tailed recognition. Long-tailed recognition addresses skewed class distributions in visual datasets. Early work explored re-weighting and resampling [9, 42, 52], decoupled classifier learning [30], and balanced normalization [51]. Recent approaches advance toward structure-aware learning capturing shared semantics among head and tail classes [12, 13], augmenting rare categories via language-driven generation [68], or optimizing distillation for long-tailed transformers [50]. These studies highlight long-tailed imbalance involves both statistical and semantic disparities in representation space. In medical imaging, similar challenges arise under data scarcity and rare disease variability. Fine-grained prototype learning [70], hybrid self-distillation [57], and curriculum-based or subtype-aware learning [27, 43] address rare category representation. However, these methods remain class-centric, overlooking the compositional semantics within images where multiple visual attributes co-occur with unequal frequency. We extend this perspective by introducing SCI, a descriptor-level fairness issue capturing the unequal co-occurrence of interpretable visual concepts within and across classes.

Fairness and subgroup robustness. Fairness-aware learning approaches such as GroupDRO [53] and domain reweighting [25, 44] mitigate disparities across predefined demographic or domain subgroups. In dermatology, [19, 35] evaluate performance gaps across skin tones and demographic groups. Beyond demographic bias, recent works address robustness under long-tailed or shifted distributions. For instance, Cui et al. [8] demonstrates unequal per-class accuracy even in balanced data, while Yue et al. [66] and Truong et al. [62] reduce head–tail bias via fairness regularization and contrastive attention. These methods rely on fixed subgroup definitions and overlook finer semantic disparities. In medical imaging, fairness mitigation often fails under domain shifts [65, 71], and approaches such as representation decorrelation or fine-tuning [10, 14] only partially address demographic bias. Long-tailed benchmarks including CXR-LT [24], LTCXNet [26], and FairMedFM [29] reveal persistent subgroup disparities despite reweighting. However, these methods depend on explicit subgroup labels and overlook semantic fairness—performance disparities across visual or diagnostic descriptors that are independent of class or demographics. We address this gap through the proposed CDI, which measures fairness in terms of semantic coverage–performance alignment.

Concept-based and interpretable models. Recent studies integrate interpretability into deep models through concept-based reasoning. Concept Bottleneck Models [37], ACE [18], and MONET [33] use human-understandable

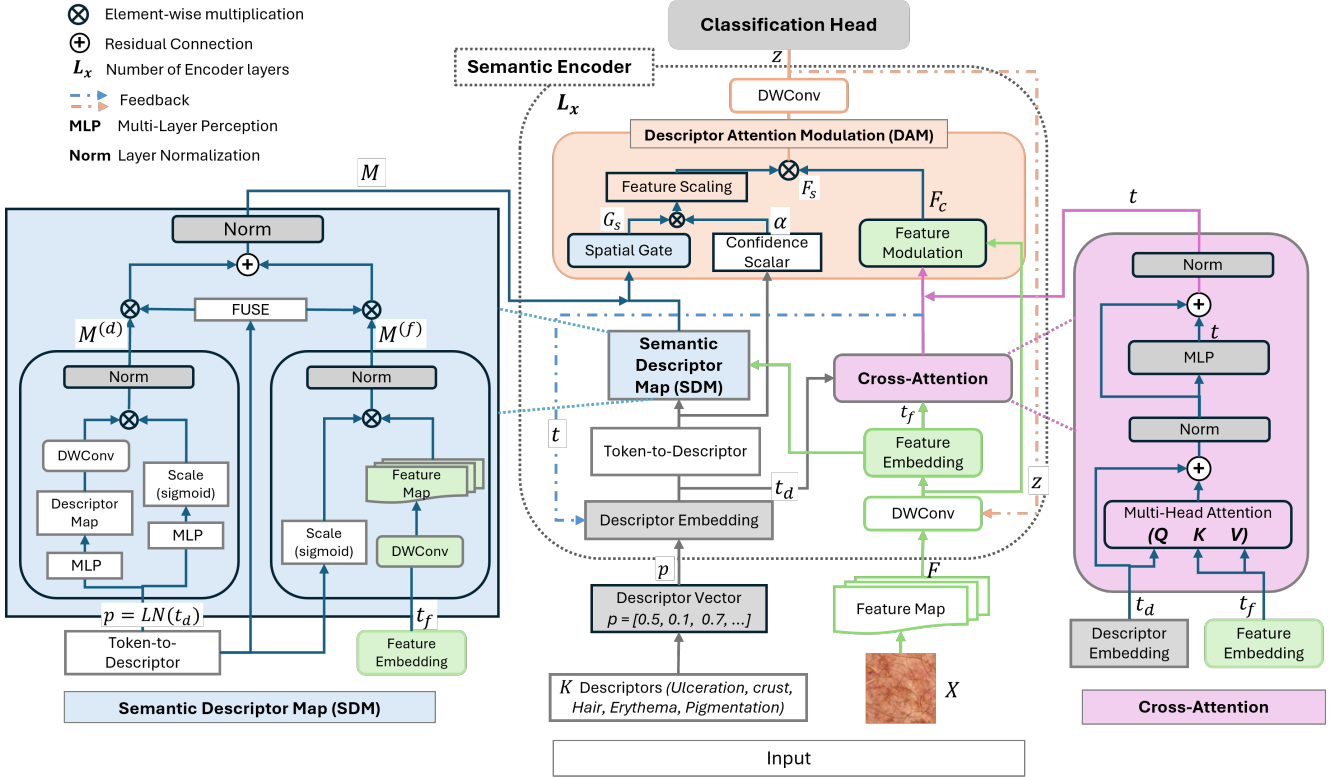


Figure 2. Overview of SemCovNet architecture. Given an image and its descriptor probabilities, the SDM (left) fuses descriptor priors and visual features into semantic attention maps. The DAM (centre) applies descriptor-conditioned channel modulation. A descriptor token, refined through Cross-Attention (right), reproduces semantic details by updating descriptor priors. Semantic Encoder alternates between SDM generation, DAM modulation, and token attention, forming a closed loop that aligns descriptor coverage with prediction confidence.

concepts for supervision or explanation. Language-guided bottlenecks [56, 64] connect high-level semantics with visual features, while sparse and generative extensions [4, 5, 46] improve alignment and interpretability. In medical imaging, concept-based methods [16, 23] address bias through meta-learning and generative augmentation. Although these approaches enhance transparency, they assume uniformly represented semantics and overlook descriptor rarity and uneven descriptor-level coverage. In contrast, our SDM and DAM modules integrate descriptor information into the representation, enabling semantic awareness of coverage imbalance.

Calibration and reliability. Confidence-based calibration metrics such as ECE [21] and its extensions [41, 54] assess the alignment between predicted confidence and accuracy, while selective prediction frameworks [17] evaluate reliability through confidence-based abstention. Recent studies [55, 59] show that deep networks remain poorly calibrated under class imbalance and distribution shifts, with reliability gaps across architectures and domains. Although fairness-aware calibration methods [20, 61] reveal subgroup-specific variations in confidence quality, they op-

erate at the prediction level and overlook disparities in semantic representation. In contrast, CDI complements traditional calibration by explicitly connecting semantic coverage to model performance, providing a descriptor-level fairness diagnostic beyond confidence reliability.

3. Methodology

3.1. Problem Setup

Given an image $x \in \mathbb{R}^{C \times H \times W}$ (C , H , and W represent channel, height, and width, respectively) and a corresponding soft semantic descriptor vector $p \in [0, 1]^K$ representing the probabilities of K interpretable concepts (e.g., attributes from MONET). Our goal is to learn a classifier $f_\theta(x, p)$ that predicts T target label $y \in \{1, \dots, T\}$ while ensuring fairness under SCI. To characterize SCI, we define Semantic Coverage Group (SCG) as unique combinations of class, descriptor, and subgroup attributes as $g = (c = \text{class}, d = \text{descriptor}, d = \text{subgroup})$. Here, *class* c refers to the primary prediction category, and *descriptor* d denotes interpretable visual semantic concepts (e.g., texture, geometry, color patterns, or lesion patterns), and

subgroup s represents demographic or contextual attributes (e.g., skin tone, sex, age, or acquisition domain). Semantic fairness is achieved when performance remains consistent across SCGs, independent of their training coverage. We define CDI = $|\rho(c_g, e_g)|$, where c_g is group-wise coverage and e_g is the miss rate (1-TPR), and $\rho(\cdot)$ is the Pearson correlation.

3.2. Semantic Encoder

Semantic Descriptor Map (SDM). The SDM module generates descriptor-specific spatial attention maps that localize semantic concepts within the feature space. It fuses descriptor-based semantic cues derived from the descriptor vector with feature-based visual activations extracted from the image, producing a unified multi-channel spatial map and each channel spatially represents the relevance of a specific descriptor.

Given an input image x , we can obtain its visual feature $F \in \mathbb{R}^{C_f \times H_f \times W_f}$ by a vision backbone, such as EfficientNet. Here, C_f , H_f , and W_f represent channel, height, and width of the feature maps, respectively. The semantic descriptor vector p is obtained by passing the image x through the MONET. The descriptor-driven SDM $M^{(d)}$ generates a prior spatial distribution independent of the input image by conditioning on the semantic descriptor p :

$$M^{(d)} = \phi_d(\psi_d(p)) \odot \sigma(W_d p) \quad (1)$$

where $\psi_d(\cdot)$ is an MLP projection that expands the descriptor embedding into a spatial representation, $\phi_d(\cdot)$ denotes a convolutional refinement network that learns descriptor-specific spatial patterns, and W_d provides a gating vector that scales each semantic channel by descriptor confidence. This enables the model to inject concept-level priors, derived from interpretable descriptors, into the visual feature space before attention-based fusion.

Similarly, the visual feature-driven SDM $M^{(f)}$ is generated by modulating spatial activations with descriptor-dependent scaling from the image feature embedding F :

$$M^{(f)} = \phi_f(F) \odot \sigma(W_s p) \quad (2)$$

where $\phi_f(\cdot)$ refines convolutional refinement network that projects F into K descriptor-specific channels, and W_s represents a descriptor gating vector that scales each semantic channel according to descriptor confidence. The Semantic Descriptor Map (SDM) M is obtained by fusing descriptor-conditioned and visual feature-conditioned representations as:

$$M = g(p) \odot M^{(f)} + (1 - g(p)) \odot M^{(d)} \quad (3)$$

where $g(p) = \sigma(\text{MLP}(p))$ is an adaptive gating function that balances the contributions of descriptor- and feature-derived information. The resulting maps are normalized and used to guide feature modulation, allowing the SDM to

adapt spatial attention based on both descriptor confidence and visual feature responses.

Cross-Attention. Each encoder layer integrates descriptor-token reasoning and spatial modulation through a descriptor-aware Cross-Attention mechanism. The descriptor token $t_d = \psi_d(p)$ attends to image patch tokens $t_f = \text{PatchTokens}(F)$ derived from the feature map F and pass into a Multi-Head Attention (MHA):

$$t = \text{MHA}(Q=t_d, K=t_f, V=t_f) + t_d \quad (4)$$

followed by a feed-forward projection and layer normalization. This interaction allows the descriptor token to aggregate context from semantically relevant spatial regions. The updated token is further projected to produce a descriptor representation that regenerates SDM. This establishes a closed feedback loop between semantic reasoning and spatial attention.

Descriptor Attention Modulation (DAM). The DAM integrates descriptor priors into the visual feature space through a combination of channel-wise FiLM [47] modulation and uncertainty-aware spatial gating.

Channel-wise Modulation. A cross-attention token $t \in \mathbb{R}^D$ (D -token dimension) which encodes semantic context refined through interaction with visual features, DAM applies t token to modulate the visual feature map F :

$$F_c = \text{BatchNorm}(F) \odot (1 + \tanh(\gamma(t))) + \beta(t), \quad (5)$$

where $\gamma(\cdot)$ and $\beta(\cdot)$ are MLPs mapping t to per-channel scale and bias parameters.

Spatial Modulation. From the SDM module, a spatial gate $G_s = \sigma(\psi(M))$ is computed via $\psi(\cdot)$ a 1×1 convolution to highlight descriptor-relevant regions. Descriptor uncertainty is estimated as $u = 4p(1 - p) \in [0, 1]^K$, which measures normalized variance under the Bernoulli distribution [15, 31], providing a simple measure of descriptor confidence dispersion. The mean uncertainty $\bar{u} = \frac{1}{K} \sum_{k=1}^K u_k \in [0, 1]$ modulates the gate strength through $\alpha = \sigma(s(1 - \bar{u}) + b)$, where (s, b) are the scale and bias learnable parameters. The final uncertainty-tempered modulation F_s is:

$$F_s = \phi(F_c \odot (0.5 + \alpha G_s)) \quad (6)$$

where $\phi(\cdot)$ is a convolutional refinement network. Descriptors with high confidence (low uncertainty) amplify spatial attention, while uncertain ones are adaptively suppressed to improve stability and robustness.

3.3. Classification Head

After the final encoder layer, an adaptive average pooling (AAP) operation produces a feature vector, which is then flattened $z = \text{AAP}(F_S) \in \mathbb{R}^D$. The classification head predict logit $\hat{y} \in \mathbb{R}^T$ of T target class, and a descriptor head

predicts the logits $\hat{p} \in \mathbb{R}^K$ of K semantic descriptor as:

$$\hat{y} = \text{LN}(z), \quad \hat{p} = \text{LN}(z)$$

where $\text{LN}(\cdot)$ denotes a Linear Layer.

3.4. Training Objective

Descriptor–Vision Alignment (DVA) Contrastive Loss. To align visual and semantic embeddings, a DVA contrastive objective is defined. Let $v = \text{Norm}(z)$ is the normalized visual feature and $d = \text{Norm}(\text{LN}(p))$ the projected descriptor embedding. The similarity matrix is computed as $S = v \cdot d^\top / \tau$, where τ is a learnable temperature. The loss is defined:

$$\mathcal{L}_{\text{DVA}} = \text{CE}(S, I), \quad (7)$$

where CE cross-entropy loss. This promotes semantic–visual consistency and improves transfer to novel descriptor domains.

Coverage Disparity Index (CDI) Regularization (\mathcal{R}_{CDI}). To reduce bias from unbalanced descriptor coverage, the CDI penalizes correlation $\text{Corr}(\cdot)$ between training coverage $c_g = \frac{1}{\mathcal{N}_g} \sum_{i \in g} p_i^{(d_g)}$ and group-wise error $e_g = 1 - \text{TPR}_g$, where TPR_g is Total Positive Rate and $p_i^{(d_g)}$ is the probability of the descriptor associated with g , and \mathcal{N}_g total samples of SCG g :

$$\text{TPR}_g = \frac{1}{\mathcal{N}_g} \sum_{i \in \mathcal{N}_g} (y_i \sigma(\hat{y}_i) + (1 - y_i) [1 - \sigma(\hat{y}_i)]), \quad (8)$$

$$\mathcal{L}_{\text{CDI}} = \left| \frac{1}{\mathcal{N}_{\text{SCG}}} \sum_g \text{Corr}(c_g, e_g) \right|, \quad (9)$$

where \mathcal{N}_{SCG} is the total SCGs, and y ground truth. \mathcal{R}_{CDI} decorrelates error from semantic coverage, encouraging more uniform error rates across SCGs and supporting semantic fairness during learning.

Joint Objective. The overall training loss ($\mathcal{L}_{\text{total}}$) combines classification accuracy, semantic grounding, descriptor–visual alignment, and coverage-aware fairness:

$$\mathcal{L}_{\text{cls}} = \text{CE}(\hat{y}, y), \quad (10)$$

$$\mathcal{L}_{\text{desc}} = \text{BCEWithLogits}(\hat{p}, p), \quad (11)$$

$$\mathcal{L}_{\text{total}} = \mathcal{L}_{\text{cls}} + \lambda_{\text{desc}} \mathcal{L}_{\text{desc}} + \lambda_{\text{dva}} \mathcal{L}_{\text{DVA}} + \lambda_{\text{cdi}} \mathcal{L}_{\text{CDI}}. \quad (12)$$

where $\lambda_{\text{desc}}, \lambda_{\text{dva}}, \lambda_{\text{cdi}}$ are the weighting to balance the task accuracy, semantic interpretability, and coverage-aware fairness.

4. Experiments

4.1. Experiment Setup

Experiment datasets. We evaluate SemCovNet on two datasets [1, 48] to analyze SCI under different class distributions for melanoma (MEL) vs. non-melanoma (NON-MEL)

classification. MILK10k [48] is a highly class-imbalanced dataset (MEL:NON-MEL $\approx 1:10$) containing 10,480 paired clinical and dermoscopic images from 5,240 lesions. Each image is annotated with MONET-derived descriptor probabilities (*ulceration/crust, hair, vasculature, erythema, pigmentation, gel/liquid, skin markings*), capturing 7 semantic cues ($K = 7$) used in dermatological diagnosis. ISIC-DICM-17K [1] is a balanced dataset (MEL:NON-MEL = 1:1) of 17,060 dermoscopic images. Descriptor probabilities for the same 7 concepts are automatically generated using a pre-trained MONET [33], providing confidence scores in $[0, 1]$ for descriptor presence. Both datasets are split into 70:10:20 for training, validation, and testing. We apply group-stratified random K-fold cross-validation based on patient IDs to prevent data leakage across splits. Regardless of overall class balance, we define SCGs as $g = (\text{class} \times \text{descriptor} \times \text{subgroup})$, showing persistent descriptor-level imbalance across attributes such as site, sex, and age. For our experiments, we consider 2 classes, 7 descriptors, and 8 anatomical sites as subgroups, forming 112 SCGs, a structured semantic space for analyzing SCI.

Implementation details. We employ EfficientNet-B0 [58] pretrained on ImageNet as the visual backbone, followed by a Semantic Encoder integrating the proposed SDM and DAM modules. Each stage performs cross-attention between descriptor tokens and visual features. SemCovNet and baseline models are trained under identical settings for fair comparison. They were trained with image sizes=224×224 pixels, epochs=50 and batch_size=32. Adam [34] optimizers and image augmentation [22] were employed. We adopted a cosine annealing schedule with one warm-up epoch [40]. Each model was tuned for the initial learning rate for the cosine cycle, ranging from 1×10^{-4} to 3×10^{-4} . During the warm-up epoch, the learning rate is set to 10 times smaller than the initial learning rate. Early stopping was applied if the AUC [45] does not change for 10 epochs, to ensure each model converged optimally. All experiments are implemented in PyTorch and trained on a single NVIDIA 2080 GPU. The loss weights were set to $\lambda_{\text{desc}} = 0.05$, $\lambda_{\text{dva}} = 0.1$, and $\lambda_{\text{cdi}} = 0.1$.

Baselines and Evaluation Metrics. We compare SemCovNet with representative baselines, EfficientNet-B0 (ENet-B0) [58] and ViT [11] for standard classification, as well as imbalance-aware methods such as Class-Balanced Loss (CBL) [9] and Asymmetric Loss (ASL) [52], the fairness-aware GroupDRO [53], and concept-based models CLIP [49] and MONET [33]. These baselines address imbalance, uncertainty, and concept alignment, enabling a fair assessment of SCI’s impact on both reliability and fairness. Performance is evaluated using AU-ROC and PR–AUC for discriminative ability under imbalance, and Sens. @ 95% Spec (Sensitivity at $\geq 95\%$ Specificity) to assess sensitivity for rare or under-covered de-

Table 1. Performance on MILK10k Dermoscopic and Clinical datasets ($\approx 1:10$ class-imbalanced). AUROC (AUC), PR-AUC (PRA), Sens. @95%Spec (S@95), Balanced Accuracy (BAcc), Macro-F1 (M-F1), and Expected Calibration Error (ECE). Results are reported at the best epoch. The best results are highlighted in bold.

Model	Dermoscopic						Clinical					
	AUC↑	PRA↑	S@95↑	BAcc↑	M-F1↑	ECE↓	AUC↑	PRA↑	S@95↑	BAcc↑	M-F1↑	ECE↓
ENet-B0	0.9114	0.5763	0.5778	0.7503	0.7490	0.0386	0.9151	0.5459	0.5222	0.6345	0.6714	0.0096
ViT	0.9032	0.4852	0.4000	0.6701	0.6887	0.0400	0.8839	0.4146	0.3667	0.5686	0.5970	0.0219
ENet-B0+CBL	0.9091	0.5662	0.5556	0.7392	0.7404	0.0203	0.9087	0.5245	0.4778	0.7350	0.7270	0.0351
ENet-B0+ASL	0.7201	0.2670	0.2889	0.5493	0.5661	0.0675	0.6128	0.1243	0.0667	0.5614	0.5608	0.0567
GroupDRO	0.8733	0.4913	0.4889	0.7582	0.6806	0.0352	0.8658	0.3921	0.4111	0.8116	0.6353	0.0576
CLIP	0.9125	0.5436	0.5556	0.6392	0.6876	0.0219	0.8855	0.5207	0.4778	0.6014	0.6424	0.0162
MONET	0.9132	0.5832	0.5778	0.7307	0.7403	0.0128	0.9071	0.5500	0.5778	0.6236	0.6711	0.0230
SemCovNet (ours)	0.9049	0.5991	0.6222	0.7874	0.7573	0.0174	0.9028	0.5698	0.5900	0.6986	0.7305	0.0759

Table 2. Results on the ISIC-DICM-17K dataset (1:1 class-balanced). SemCovNet demonstrates descriptor-level fairness and sensitivity, even under balanced conditions, showing robustness against class distribution bias. The best results are in bold.

Model	AUC↑	PRA↑	S@95↑	BAcc↑	M-F1↑	ECE↓
ENet-B0	0.8612	0.7730	0.3802	0.7600	0.7646	0.0613
ViT	0.8098	0.7182	0.2937	0.6675	0.6725	0.0410
ENet-B0+CBL	0.8612	0.7730	0.3802	0.7600	0.7646	0.0613
ENet-B0+ASL	0.7543	0.6569	0.2605	0.6591	0.6634	0.2047
GroupDRO	0.8557	0.7632	0.3881	0.7479	0.7542	0.1118
CLIP	0.8525	0.7839	0.3855	0.7546	0.7560	0.0565
MONET	0.8598	0.7900	0.4030	0.7653	0.7650	0.0661
SemCovNet (ours)	0.8822	0.8098	0.4138	0.7893	0.7855	0.0421

scriptors. Balanced Accuracy and Macro-F1 measure class-level robustness, while Expected Calibration Error (ECE) quantifies prediction reliability. Fairness is analyzed using the CDI, the correlation between semantic coverage and error (1-TPR) across SCGs. Together, these metrics evaluate both recognition performance and semantic fairness, highlighting the benefits of coverage-aware learning.

4.2. Comparative Performance Analysis

Imbalanced settings. On the MILK10k dataset, Table 1 shows that standard models (ENet-B0, ViT) achieve high AUROC but exhibit strong bias toward class-frequency, resulting in poor sensitivity for underrepresented class. Imbalance- and fairness-aware methods (CBL, GroupDRO) improve sensitivity marginally but only reweight by class frequency, overlooking descriptor-level disparities. Concept-based models (CLIP, MONET) enhance interpretability, however, fail to disentangle coverage–error correlation due to their lack of explicit descriptor–feature alignment. SemCovNet incorporates semantic descriptors via SDM and refines them through feedback and CDI regularization, enabling explicit alignment between visual and semantic spaces. This achieves the highest

Sens. @95%Spec and Macro-F1 across both dermoscopic and clinical modalities, improving sensitivity by +1.22 to 4.4% and Macro-F1 by +0.6% on average, while maintaining low calibration error. Moreover, SemCovNet remains robust even under soft, uncertain descriptors, demonstrating stable generalization across modalities and descriptor coverage ranges.

Balanced settings. On the class balanced ISIC-DICM-17K dataset (Table 2), traditional and imbalance-aware baselines converge, demonstrating their influence on class reweighting. However, descriptor-level imbalance persists—models still prefer frequent descriptors. GroupDRO improves minority subgroups coarsely, while CLIP and MONET transfer static semantic priors without adaptive refinement. In contrast, SemCovNet continues to outperform all baselines, achieving +1.1 to 4.8% higher Sens. @95%Spec and +2.05 to 5.9% Macro-F1, with comparable calibration (ECE). These consistent gains indicate that SCI persists beyond class imbalance and that descriptor-aware reasoning is essential for fairness even in balanced class settings.

4.3. Fairness Analysis

We further assess descriptor-level fairness using the Coverage Disparity Index (CDI), which asks: *Do SCGs with low training coverage also show higher error rates?* \mathcal{R}_{CDI} penalizes this correlation during training, quantifying fairness across SCGs rather than relying on class-level frequency or coverage thresholds. CDI, TPR_w (the minimum true-positive rate across SCGs), and TPR_{std} (the standard deviation of per-SCG TPRs) evaluate the uniformity of performance across descriptors, where lower CDI and TPR_{std} and higher TPR_w indicate fairer performance. Table 3 results show that ENet-B0 and ViT exhibit high CDI, indicating bias toward dominant coverage SCGs. CB Loss and ASL mitigate class imbalance but not semantic disparity; GroupDRO applies global parity, however, misses descriptor-specific bias; CLIP and MONET leverage semantics without adaptive alignment, producing uneven per-

Table 3. Fairness comparison on MILK10k (Dermoscopic and Clinical; 1:10 class-imbalanced) and ISIC-DICM-17K (1:1 class-balanced) datasets. CDI (coverage–error correlation), TPR_w (minimum per-SCG TPR; weakest SCG), and TPR_{std} (standard deviation of per-SCG TPR) quantify semantic fairness. Lower CDI and TPR_{std} and higher TPR_w indicate more uniform performance across SCGs. Δ computed w.r.t. the best baseline and highlighted in bold.

Model	MILK10k (Dermoscopic)			MILK10k (Clinical)			ISIC-DICM-17K		
	CDI \downarrow (Δ)	$TPR_w\uparrow$	$TPR_{std}\downarrow$	CDI \downarrow (Δ)	$TPR_w\uparrow$	$TPR_{std}\downarrow$	CDI \downarrow (Δ)	$TPR_w\uparrow$	$TPR_{std}\downarrow$
ENet-B0	0.6210	0.7333	0.0579	0.7834	0.1667	0.1382	0.2833	0.2500	0.0801
ViT	0.9454	0.3333	0.0594	0.8497	0.2000	0.0838	0.2940	0.0000	0.1210
ENet-B0+CB Loss	0.9584	0.1667	0.1088	0.8943	0.2667	0.1374	0.4131	0.5854	0.1050
ENet-B0+ASL	0.8417	0.0833	0.0735	0.7641	0.5000	0.0633	0.3053	0.0000	0.2100
GroupDRO	0.4661	0.4167	0.1490	0.2081	0.8333	0.0618	0.2975	0.5000	0.1322
CLIP	0.4017	0.0667	0.3500	0.2801	0.2000	0.2934	0.4773	0.0000	0.2537
MONET	0.3261	0.2500	0.2790	0.3215	0.0833	0.3284	0.4188	0.7049	0.0912
SemCovNet (ours)	0.0616(-0.26)	0.2667	0.2601	0.1918(-0.02)	0.1667	0.2891	0.2397(-0.04)	0.7500	0.0666

Table 4. Ablation of SDM variants, keeping all other modules constant. *Hybrid* denotes fuse Descriptor–Only and Feature–Only variant using additive $+$, multiplicative \times , or gated \odot operations.

SDM Variant	AUC \uparrow	S@95 \uparrow	CDI \downarrow
Descriptor-Only	0.8653 \pm 0.008	0.4148 \pm 0.026	0.1164 \pm 0.065
Feature-Only	0.8591 \pm 0.004	0.4185 \pm 0.032	0.1451 \pm 0.045
Hybrid $_{+}$	0.8614 \pm 0.005	0.3778 \pm 0.009	0.1169 \pm 0.016
Hybrid $_{\times}$	0.8674 \pm 0.006	0.4407 \pm 0.023	0.1429 \pm 0.015
Hybrid \odot	0.8600 \pm 0.002	0.4592 \pm 0.064	0.0986 \pm 0.012

SCG sensitivities. SemCovNet achieves the lowest CDI and TPR_{std} and the highest TPR_w across datasets, reducing CDI by $\approx 45\%$ on average (up to 81% on MILK10k Dermoscopic) and increasing TPR_w by +0.09 on average. These results demonstrate that SemCovNet effectively decouples coverage and error, establishing descriptor-level fairness under both imbalanced and balanced conditions.

4.4. Ablation Study

We conduct extensive ablations to disentangle the design choices vary the descriptor–feature conditioning mode, the interaction between attention and descriptor–feature modulation, and Coverage–Error for semantic fairness. Experiments are evaluated using reliability and CDI metrics to demonstrate how architectural factors affect fairness–performance trade-offs.

Descriptor conditioning strategy. We compare descriptor-driven, feature-driven, and hybrid SDM modes on the MILK10k Clinical dataset to analyze how semantic attributes contribute to coverage–error alignment. While explicit descriptor conditioning (Descriptor-Only) improves performance, it can reduce contextual flexibility. Conversely, Feature-Only relies on visual representations, often overlooking the semantics of descriptors. The hybrid design adaptively fuses descriptor and feature attributes, achieving the best trade-off between accuracy and fairness, with higher sensitivity and the lowest CDI. Table 4 results show

Table 5. Ablation of Cross-Attention (attn) ∞ DAM order, keeping other modules constant. *Mixture* denotes gated fusion between the two modules. $Mixture_{attn \rightarrow DAM}$ and $Mixture_{DAM \rightarrow attn}$ denotes swap the attn \rightarrow DAM and DAM \rightarrow attn ordering between early and late layers in Semantic Encoder.

	Order	AUC \uparrow	S@95 \uparrow	CDI \downarrow
Dermoscopic	attn \rightarrow DAM	0.8977 \pm 0.013	0.5741 \pm 0.050	0.3447 \pm 0.025
	DAM \rightarrow attn	0.8931 \pm 0.008	0.5592 \pm 0.021	0.3172 \pm 0.038
	$Mixture_{attn \rightarrow DAM}$	0.9011 \pm 0.007	0.5741 \pm 0.055	0.1474 \pm 0.044
	$Mixture_{DAM \rightarrow attn}$	0.9096 \pm 0.011	0.6222 \pm 0.033	0.0777 \pm 0.035
	Mixture	0.8948 \pm 0.014	0.6074 \pm 0.055	0.3172 \pm 0.061
Clinical	attn \rightarrow DAM	0.8900 \pm 0.008	0.5037 \pm 0.010	0.1752 \pm 0.096
	DAM \rightarrow attn	0.8711 \pm 0.005	0.4519 \pm 0.014	0.1311 \pm 0.090
	$Mixture_{attn \rightarrow DAM}$	0.8691 \pm 0.001	0.3963 \pm 0.028	0.0778 \pm 0.007
	$Mixture_{DAM \rightarrow attn}$	0.8692 \pm 0.008	0.4296 \pm 0.037	0.0897 \pm 0.084
	Mixture	0.8737 \pm 0.005	0.4185 \pm 0.026	0.1771 \pm 0.126

that among all variants, the Hybrid \odot (gated fusion) demonstrates the most balanced improvement—enhancing sensitivity by +10.7% and reducing CDI by 15% relative to the descriptor-only variant, demonstrating adaptive gating effectively harmonizes contextual and semantic modulation.

Cross-Attention ∞ DAM interaction. We investigate the impact of sequencing between Cross-Attention (attn) and DAM on performance across Dermoscopic and Clinical modalities in MILK10k. Descriptor probabilities from MONET are typically high-confidence for dermoscopic and low-confidence (soft) for clinical images, leading to different optimal reasoning flows. When cross-attention precedes DAM (attn \rightarrow DAM), descriptor tokens attend to unmodulated visual features, reducing bias from uncertain descriptor priors and improving robustness under domain shift. Conversely, when DAM precedes attention (DAM \rightarrow attn), the descriptors act as spatial priors that highlight lesion-relevant regions early, which is beneficial when the descriptors are reliable and visually well-localized.

We evaluate five configurations within each Semantic

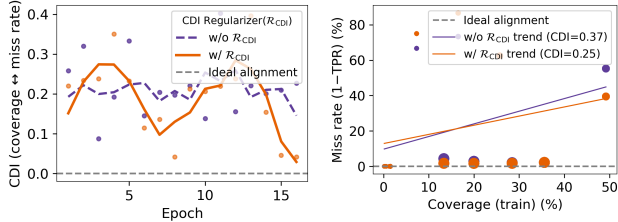


Figure 3. Semantic Coverage–Error $w/$ and w/o CDI Regularizer (R_{CDI}) on MILK10k (Dermoscopic). (Left) The CDI statistic progressively decays toward zero during training, indicating effective coverage–error decoupling. (Right) R_{CDI} reduces CDI demonstrating improved semantic fairness.

Table 6. Semantic grounding and visual reasoning on MILK10k (Dermoscopic). Improvements ($\Delta S@95_{tail}$) in low-coverage (bottom 30%) SCGs and higher descriptor–vision alignment scores (Align-cos, R@1) indicate stronger semantic grounding and better recognition of rare descriptors. Δ computed w.r.t. the Visual-only as baseline.

Method	$S@95_{tail}(\Delta) \uparrow$	Align-cos \uparrow	R@1 \uparrow
Visual-only	0.1222 (+0.000)	-0.0372	0.0325
SDM	0.2444 (+0.122)	0.0229	0.0074
SDM+DVA (Ours)	0.3667 (+0.245)	0.7862	0.8401

Encoder layer: (i) attn→DAM, where global attention precedes semantic modulation; (ii) DAM→attn, where descriptors guide early spatial focus; (iii–iv) Mixture_{attn}→DAM and Mixture_{DAM}→attn, which swap the ordering between early and late layers; and (v) Mixture, which fuses both orderings within each layer via learned gating. Table 5 results show that the Mixture_{DAM}→attn configuration achieves the highest dermoscopic performance, indicating that early descriptor modulation is most effective when descriptors are confident and spatially consistent. For the clinical modality, where descriptor signals are weaker and more uncertain, attn→DAM performs best as attending to unmodulated features first preserves contextual reliability.

Effectiveness of CDI Regularization (R_{CDI}). We analyse the impact of the proposed R_{CDI} on training dynamics and fairness on the MILK10k (Dermoscopic) dataset. Figure 3 visualises the CDI trajectory across training epochs. The correlation steadily approaches zero only when R_{CDI} is active. It shows that the regularizer effectively reduces coverage–error correlation (CDI↓).

Semantic Grounding and Visual Reasoning Analysis.

We evaluate semantic grounding and cross-modal reasoning by comparing Visual-only, SDM, and SDM+DVA, which aligns descriptor embeddings with visual features. Grounding is quantified using Align-cos (descriptor–image cosine similarity) and R@1, while fairness on low-coverage (tail) descriptors is measured by $\Delta S@95_{tail}$ over the bottom 30%

coverage SCGs. Table 6 results show the improvement on descriptor–vision alignment leads to significant gains in tail performance. SDM+DVA achieves $+0.245 \Delta S@95_{tail}$, along with higher Align-cos (+0.82) and R@1 (+0.81) over Visual-only, indicating stronger grounding and better recognition of rare descriptors. Moreover, SDM reduces the dermoscopic↔clinical (MILK10k) alignment gap (0.026 → 0.009), with the largest tail improvement in the clinical domain, where descriptors are uncertain. The progression *Visual-only* → *SDM* → *SDM+DVA* shows that stronger semantic alignment directly improves tail sensitivity, reduces domain bias, and achieves descriptor-level fairness under SCI.

5. Discussion and Conclusion

This work establishes Semantic Coverage Imbalance (SCI) as a fundamental and previously overlooked source of unfairness in visual recognition. Unlike prior studies that treat coverage as a representative for class diversity, we formalize SCI as the *quantitative mismatch between descriptor-level training representation and descriptor-specific performance*. By grounding fairness in interpretable semantic descriptors rather than class frequencies, SCI provides an approach to analyze representational bias beyond demographic or class imbalance. The proposed SemCovNet framework embeds SCI into model learning through Semantic Descriptor Maps (SDM) and Descriptor Attention Modulation (DAM), enabling adaptive alignment between visual and semantic spaces. The Descriptor–Visual Alignment (DVA) objective aligns between descriptor attention and visual evidence, while the Coverage Disparity Index (CDI) quantifies semantic fairness by coverage–performance alignment. Together, these components create a closed-loop mechanism that identifies underrepresented semantics, descriptor reasoning, and mitigates bias at the visual concept level. Empirical results on MILK10k and ISIC-DICM-17K demonstrate that SemCovNet consistently improves sensitivity on rare descriptors while maintaining balanced performance. In conclusion, this framework integrates semantic interpretability and fairness, providing a new perspective on fair and coverage-aware representation learning in vision models. Our formulation of SCI is demonstrated within dermatological lesion classification using MONET-derived descriptors, which may limit its immediate generality to other domains. However, the principle of modeling and correcting descriptor-level coverage imbalance is applicable to tasks involving interpretable concepts such as radiology, pathology, and fine-grained visual reasoning.

References

[1] Sakib Ahammed, Xia Cui, Wenqi Lu, and Moi Hoon Yap. Skin lesion classification using dermoscopic images and clinical metadata: Insights from multimodal models. In *Proceedings of the Computer Vision and Pattern Recognition Conference (CVPR) Workshops*, pages 222–230, 2025. 5

[2] Shaden Alshammari, Yu-Xiong Wang, Deva Ramanan, and Shu Kong. Long-tailed recognition via weight balancing. In *Proceedings of the IEEE/CVF conference on computer vision and pattern recognition*, pages 6897–6907, 2022. 2

[3] Giuseppe Argenziano, Gabriella Fabbrocini, Paolo Carli, Vincenzo De Giorgi, Elena Sammarco, and Mario Delfino. Epiluminescence microscopy for the diagnosis of doubtful melanocytic skin lesions: comparison of the abcd rule of dermatoscopy and a new 7-point checklist based on pattern analysis. *Archives of dermatology*, 134(12):1563–1570, 1998. 1

[4] Itay Benou and Tammy Riklin Raviv. Show and tell: Visually explainable deep neural nets via spatially-aware concept bottleneck models. In *Proceedings of the Computer Vision and Pattern Recognition Conference*, pages 30063–30072, 2025. 3

[5] Usha Bhalla, Alex Oesterling, Suraj Srinivas, Flavio Calmon, and Himabindu Lakkaraju. Interpreting clip with sparse linear concept embeddings (splice). *Advances in Neural Information Processing Systems*, 37:84298–84328, 2024. 3

[6] Noel Codella, Veronica Rotemberg, Philipp Tschandl, M Emre Celebi, Stephen Dusza, David Gutman, Brian Helba, Aadi Kalloo, Konstantinos Liopyris, Michael Marchetti, et al. Skin lesion analysis toward melanoma detection 2018: A challenge hosted by the international skin imaging collaboration (isic). *arXiv preprint arXiv:1902.03368*, 2019. 1

[7] Elliot Creager, Jörn-Henrik Jacobsen, and Richard Zemel. Environment inference for invariant learning. In *International Conference on Machine Learning*, pages 2189–2200. PMLR, 2021. 2

[8] Jiequan Cui, Beier Zhu, Xin Wen, Xiaojuan Qi, Bei Yu, and Hanwang Zhang. Classes are not equal: An empirical study on image recognition fairness. In *Proceedings of the IEEE/CVF Conference on Computer Vision and Pattern Recognition*, pages 23283–23292, 2024. 2

[9] Yin Cui, Menglin Jia, Tsung-Yi Lin, Yang Song, and Serge Belongie. Class-balanced loss based on effective number of samples. In *Proceedings of the IEEE/CVF conference on computer vision and pattern recognition*, pages 9268–9277, 2019. 2, 5

[10] Wenlong Deng, Yuan Zhong, Qi Dou, and Xiaoxiao Li. On fairness of medical image classification with multiple sensitive attributes via learning orthogonal representations. In *International Conference on Information Processing in Medical Imaging*, pages 158–169. Springer, 2023. 2

[11] Alexey Dosovitskiy, Lucas Beyer, Alexander Kolesnikov, Dirk Weissenborn, Xiaohua Zhai, Thomas Unterthiner, Mostafa Dehghani, Matthias Minderer, Georg Heigold, Sylvain Gelly, Jakob Uszkoreit, and Neil Houlsby. An image is worth 16x16 words: Transformers for image recognition at scale. *ICLR*, 2021. 5

[12] Yingxiao Du and Jianxin Wu. No one left behind: Improving the worst categories in long-tailed learning. In *Proceedings of the IEEE/CVF conference on computer vision and pattern recognition*, pages 15804–15813, 2023. 2

[13] Yingjun Du, Jiayi Shen, Xiantong Zhen, and Cees GM Snoek. Superdisco: Super-class discovery improves visual recognition for the long-tail. In *Proceedings of the IEEE/CVF conference on computer vision and pattern recognition*, pages 19944–19954, 2023. 2

[14] Raman Dutt, Ondrej Bohdal, Sotirios A Tsaftaris, and Timothy Hospedales. Fairtune: Optimizing parameter efficient fine tuning for fairness in medical image analysis. In *International Conference on Learning Representations*, 2024. 2

[15] Yarin Gal and Zoubin Ghahramani. Dropout as a bayesian approximation: Representing model uncertainty in deep learning. In *international conference on machine learning*, pages 1050–1059. PMLR, 2016. 4

[16] Mengdi Gao, Hongyang Jiang, Lei Zhu, Zhe Jiang, Mufeng Geng, Qiushi Ren, and Yanye Lu. Discriminative ensemble meta-learning with co-regularization for rare fundus diseases diagnosis. *Medical Image Analysis*, 89:102884, 2023. 3

[17] Yonatan Geifman and Ran El-Yaniv. Selectivenet: A deep neural network with an integrated reject option. In *International conference on machine learning*, pages 2151–2159. PMLR, 2019. 3

[18] Amirata Ghorbani, James Wexler, James Y Zou, and Been Kim. Towards automatic concept-based explanations. *Advances in neural information processing systems*, 32, 2019. 2

[19] Matthew Groh, Omar Badri, Roxana Daneshjou, Arash Koochek, Caleb Harris, Luis R Soenksen, P Murali Doraiswamy, and Rosalind Picard. Deep learning-aided decision support for diagnosis of skin disease across skin tones. *Nature Medicine*, 30(2):573–583, 2024. 2

[20] Sebastian Gruber and Florian Buettner. Better uncertainty calibration via proper scores for classification and beyond. *Advances in Neural Information Processing Systems*, 35: 8618–8632, 2022. 3

[21] Chuan Guo, Geoff Pleiss, Yu Sun, and Kilian Q Weinberger. On calibration of modern neural networks. In *International conference on machine learning*, pages 1321–1330. PMLR, 2017. 3

[22] Qishen Ha, Bo Liu, and Fuxu Liu. Identifying melanoma images using efficientnet ensemble: Winning solution to the siim-isic melanoma classification challenge. *arXiv preprint arXiv:2010.05351*, 2020. 5

[23] Pengxiao Han, Changkun Ye, Jieming Zhou, Jing Zhang, Jie Hong, and Xuesong Li. Latent-based diffusion model for long-tailed recognition. In *Proceedings of the IEEE/CVF conference on computer vision and pattern recognition*, pages 2639–2648, 2024. 3

[24] Gregory Holste, Yiliang Zhou, Song Wang, Ajay Jaiswal, Mingquan Lin, Sherry Zhuge, Yuzhe Yang, Dongkyun Kim, Trong-Hieu Nguyen-Mau, Minh-Triet Tran, et al. Towards long-tailed, multi-label disease classification from chest x-

ray: Overview of the cxr-lt challenge. *Medical Image Analysis*, 97:103224, 2024. 2

[25] Sangwoo Hong, Youngseok Yoon, Hyungjun Joo, and Jungwoo Lee. Gbmix: Enhancing fairness by group-balanced mixup. *IEEE Access*, 12:18877–18887, 2024. 2

[26] Chin-Wei Huang, Chi-Yu Chen, Mu-Yi Shen, Kuan-Chang Shih, Shih-Chih Lin, and Po-Chih Kuo. Ltcxnet: Tackling long-tailed multi-label classification and racial bias in chest x-ray analysis. In *MICCAI Workshop on Fairness of AI in Medical Imaging*, pages 1–10. Springer, 2025. 2

[27] Ruobing Huang, Yinyu Ye, Ao Chang, Han Huang, Zijie Zheng, Long Tan, Guoxue Tang, Man Luo, Xiuwen Yi, Pan Liu, et al. Subtyping breast lesions via collective intelligence based long-tailed recognition in ultrasound. *Medical Image Analysis*, 102:103548, 2025. 2

[28] Zhimeng Stephen Jiang, Xiaotian Han, Hongye Jin, Guanchu Wang, Rui Chen, Na Zou, and Xia Hu. Chasing fairness under distribution shift: A model weight perturbation approach. *Advances in Neural Information Processing Systems*, 36:63931–63944, 2023. 2

[29] Ruinan Jin, Zikang Xu, Yuan Zhong, Qingsong Yao, DOU QI, S Kevin Zhou, and Xiaoxiao Li. Fairmedfm: fairness benchmarking for medical imaging foundation models. *Advances in Neural Information Processing Systems*, 37:111318–111357, 2024. 2

[30] Bingyi Kang, Saining Xie, Marcus Rohrbach, Zhicheng Yan, Albert Gordo, Jiashi Feng, and Yannis Kalantidis. Decoupling representation and classifier for long-tailed recognition. In *Eighth International Conference on Learning Representations (ICLR)*, 2020. 2

[31] Alex Kendall and Yarin Gal. What uncertainties do we need in bayesian deep learning for computer vision? *Advances in neural information processing systems*, 30, 2017. 4

[32] Muhammad Osama Khan, Muhammad Muneeb Afzal, Shujaat Mirza, and Yi Fang. How fair are medical imaging foundation models? In *Machine Learning for Health (ML4H)*, pages 217–231. PMLR, 2023. 2

[33] Chanwoo Kim, Soham U Gadgil, Alex J DeGrave, Jesutofunmi A Omiye, Zhuo Ran Cai, Roxana Daneshjou, and Su-In Lee. Transparent medical image ai via an image–text foundation model grounded in medical literature. *Nature medicine*, 30(4):1154–1165, 2024. 2, 5

[34] Diederik P Kingma and Jimmy Ba. Adam: A method for stochastic optimization. *arXiv preprint arXiv:1412.6980*, 2014. 5

[35] Newton M Kinyanjui, Timothy Odonga, Celia Cintas, Noel CF Codella, Rameswar Panda, Prasanna Sattigeri, and Kush R Varshney. Fairness of classifiers across skin tones in dermatology. In *International conference on medical image computing and computer-assisted intervention*, pages 320–329. Springer, 2020. 2

[36] Alexander Kirillov, Eric Mintun, Nikhila Ravi, Hanzi Mao, Chloe Rolland, Laura Gustafson, Tete Xiao, Spencer Whitehead, Alexander C Berg, Wan-Yen Lo, et al. Segment anything. In *Proceedings of the IEEE/CVF international conference on computer vision*, pages 4015–4026, 2023. 1

[37] Pang Wei Koh, Thao Nguyen, Yew Siang Tang, Stephen Mussmann, Emma Pierson, Been Kim, and Percy Liang. Concept bottleneck models. In *International conference on machine learning*, pages 5338–5348. PMLR, 2020. 2

[38] Tiarna Lee, Esther Puyol-Antón, Bram Ruijsink, Keana Aitcheson, Miaojing Shi, and Andrew P King. An investigation into the impact of deep learning model choice on sex and race bias in cardiac mr segmentation. In *Workshop on Clinical Image-Based Procedures*, pages 215–224. Springer, 2023. 2

[39] Dong Li, Chen Zhao, Minglai Shao, and Wenjun Wang. Learning fair invariant representations under covariate and correlation shifts simultaneously. In *Proceedings of the 33rd ACM International Conference on Information and Knowledge Management*, pages 1174–1183, 2024. 2

[40] Ilya Loshchilov and Frank Hutter. Sgdr: Stochastic gradient descent with warm restarts. *arXiv preprint arXiv:1608.03983*, 2016. 5

[41] Charlie Marx, Sofian Zalouk, and Stefano Ermon. Calibration by distribution matching: Trainable kernel calibration metrics. *Advances in Neural Information Processing Systems*, 36:25910–25928, 2023. 3

[42] Aditya Krishna Menon, Sadeep Jayasumana, Ameya S Rawat, Himanshu Jain, Andreas Veit, and Sanjiv Kumar. Long-tail learning via logit adjustment. In *International Conference on Learning Representations (ICLR)*, 2021. 2

[43] Zihao Mi, Jianan Zhang, Xueyu Liu, Guanghui Yue, Jun-hong Yue, Mingqiang Wei, Yidi Li, and Yongfei Wu. Multi-instance curriculum learning for histopathology image classification with bias reduction. *Medical Image Analysis*, page 103647, 2025. 2

[44] Youssef Mroueh et al. Fair mixup: Fairness via interpolation. In *International Conference on Learning Representations*, 2021. 2

[45] Khashayar Namdar, Masoom A Haider, and Farzad Khalvati. A modified auc for training convolutional neural networks: taking confidence into account. *Frontiers in artificial intelligence*, 4:582928, 2021. 5

[46] Konstantinos Panagiotis Panousis, Dino Ienco, and Diego Marcos. Sparse linear concept discovery models. In *Proceedings of the ieee/cvf international conference on computer vision*, pages 2767–2771, 2023. 3

[47] Ethan Perez, Florian Strub, Harm de Vries, Vincent Dumoulin, and Aaron C. Courville. Film: Visual reasoning with a general conditioning layer. In *AAAI*, 2018. 4

[48] Tschandl Philipp, Akay Nisa Bengü, Rosendahl Cliff, Rotemberg Veronica, Todorovska Verche, Weber Jochen, Wolber Anna Katharina, Müller Christoph, Kurtansky Nicholas, Halpern Allan, et al. Milk10k: A hierarchical multimodal imaging learning toolkit for diagnosing pigmented and non-pigmented skin cancer and its simulators. *Journal of Investigative Dermatology*, 2025. 1, 5

[49] Alec Radford, Jong Wook Kim, Chris Hallacy, Aditya Ramesh, Gabriel Goh, Sandhini Agarwal, Girish Sastry, Amanda Askell, Pamela Mishkin, Jack Clark, et al. Learning transferable visual models from natural language supervision. In *International conference on machine learning*, pages 8748–8763. PMLR, 2021. 5

[50] Harsh Rangwani, Pradipto Mondal, Mayank Mishra, Ashish Ramayee Asokan, and R Venkatesh Babu. Deit-lt:

Distillation strikes back for vision transformer training on long-tailed datasets. In *Proceedings of the IEEE/CVF Conference on Computer Vision and Pattern Recognition*, pages 23396–23406, 2024. 1, 2

[51] Jiawei Ren, Cunjun Yu, Xiao Ma, Haiyu Zhao, Shuai Yi, et al. Balanced meta-softmax for long-tailed visual recognition. *Advances in neural information processing systems*, 33:4175–4186, 2020. 2

[52] Tal Ridnik, Emanuel Ben-Baruch, Nadav Zamir, Asaf Noy, Itamar Friedman, Matan Protter, and Lihi Zelnik-Manor. Asymmetric loss for multi-label classification. In *Proceedings of the IEEE/CVF international conference on computer vision*, pages 82–91, 2021. 2, 5

[53] Shiori Sagawa, Pang Wei Koh, Tatsunori B. Hashimoto, and Percy Liang. Distributionally robust neural networks for group shifts: On the importance of regularization for worst-case generalization. In *International Conference on Learning Representations (ICLR)*, 2020. 2, 5

[54] Tiago Salvador, Stephanie Cairns, Vikram Voleti, Noah Marshall, and Adam M Oberman. Faircal: Fairness calibration for face verification. In *International Conference on Learning Representations*, 2022. 3

[55] Abhishek Singh Sambyal, Usma Niyaz, Narayanan C Krishnan, and Deepti R Bathula. Understanding calibration of deep neural networks for medical image classification. *Computer Methods and Programs in Biomedicine*, 242:107816, 2023. 2, 3

[56] Divyansh Srivastava, Ge Yan, and Lily Weng. Vlg-cbm: Training concept bottleneck models with vision-language guidance. *Advances in Neural Information Processing Systems*, 37:79057–79094, 2024. 2, 3

[57] Jinghan Sun, Dong Wei, Liansheng Wang, and Yefeng Zheng. Hybrid unsupervised representation learning and pseudo-label supervised self-distillation for rare disease imaging phenotype classification with dispersion-aware imbalance correction. *Medical Image Analysis*, 93:103102, 2024. 2

[58] Mingxing Tan and Quoc Le. Efficientnet: Rethinking model scaling for convolutional neural networks. In *International conference on machine learning*, pages 6105–6114. PMLR, 2019. 5

[59] Linwei Tao, Younan Zhu, Haolan Guo, Minjing Dong, and Chang Xu. A benchmark study on calibration. In *International Conference on Learning Representations*, 2024. 2, 3

[60] Davoud Ataei Tarzanagh, Bojian Hou, Boning Tong, Qi Long, and Li Shen. Fairness-aware class imbalanced learning on multiple subgroups. In *Uncertainty in Artificial Intelligence*, pages 2123–2133. PMLR, 2023. 1

[61] Junjiao Tian, Yen-Cheng Liu, Nathaniel Glaser, Yen-Chang Hsu, and Zsolt Kira. Posterior re-calibration for imbalanced datasets. *Advances in neural information processing systems*, 33:8101–8113, 2020. 3

[62] Thanh-Dat Truong, Utsav Prabhu, Bhiksha Raj, Jackson Cothren, and Khoa Luu. Falcon: Fairness learning via contrastive attention approach to continual semantic scene understanding. In *Proceedings of the Computer Vision and Pattern Recognition Conference*, pages 15065–15075, 2025. 2

[63] Yue Xu, Yong-Lu Li, Jiefeng Li, and Cewu Lu. Constructing balance from imbalance for long-tailed image recognition. In *European conference on computer vision*, pages 38–56. Springer, 2022. 2

[64] Yue Yang, Artemis Panagopoulou, Shenghao Zhou, Daniel Jin, Chris Callison-Burch, and Mark Yatskar. Language in a bottle: Language model guided concept bottlenecks for interpretable image classification. In *Proceedings of the IEEE/CVF conference on computer vision and pattern recognition*, pages 19187–19197, 2023. 2, 3

[65] Yuzhe Yang, Haoran Zhang, Judy W Gichoya, Dina Katabi, and Marzyeh Ghassemi. The limits of fair medical imaging ai in real-world generalization. *Nature Medicine*, 30(10):2838–2848, 2024. 2

[66] Xinli Yue, Ningping Mou, Qian Wang, and Lingchen Zhao. Revisiting adversarial training under long-tailed distributions. In *Proceedings of the IEEE/CVF conference on computer vision and pattern recognition*, pages 24492–24501, 2024. 2

[67] Zeliang Zhang, Mingqian Feng, Zhiheng Li, and Chenliang Xu. Discover and mitigate multiple biased subgroups in image classifiers. In *Proceedings of the IEEE/CVF Conference on Computer Vision and Pattern Recognition*, pages 10906–10915, 2024. 2

[68] Qihao Zhao, Yalun Dai, Hao Li, Wei Hu, Fan Zhang, and Jun Liu. Ltgc: Long-tail recognition via leveraging llms-driven generated content. In *Proceedings of the IEEE/CVF Conference on Computer Vision and Pattern Recognition*, pages 19510–19520, 2024. 2

[69] Yukun Zhou, Mark A Chia, Siegfried K Wagner, Murat S Ayhan, Dominic J Williamson, Robbert R Struyven, Timing Liu, Moucheng Xu, Mateo G Lozano, Peter Woodward-Court, et al. A foundation model for generalizable disease detection from retinal images. *Nature*, 622(7981):156–163, 2023. 1

[70] Yongbei Zhu, Shuo Wang, He Yu, Weimin Li, and Jie Tian. Sfpl: Sample-specific fine-grained prototype learning for imbalanced medical image classification. *Medical Image Analysis*, 97:103281, 2024. 2

[71] Yongshuo Zong, Yongxin Yang, and Timothy Hospedales. Medfair: Benchmarking fairness for medical imaging. In *International Conference on Learning Representations (ICLR)*, 2023. 2

SemCovNet: Towards Fair and Semantic Coverage-Aware Learning for Underrepresented Visual Concepts

Supplementary Material

6. SemCovNet Workflow

Figure 4 shows the conceptual workflow of SemCovNet. First, samples are grouped into Semantic Coverage Groups (SCGs) by class, descriptor (concept), and subgroup (sensitive attributes). Coverage is then estimated within each SCG to identify underrepresented groups. During learning, Descriptor Attention Modulation reduces reliance on poorly covered semantic descriptors, preventing unstable predictions for rare semantics. Descriptor-Vision Alignment encourages consistent use of semantic cues and reduces sensitivity to noisy descriptor scores. After learning, errors are evaluated across SCGs. SCI occurs when errors are consistently higher in low-coverage SCGs. The Coverage Disparity Index (CDI) diagnoses this by measuring how errors depend on coverage. This diagnosis is updated during training to stabilize performance across SCGs and mitigate SCI.

7. Semantic Coverage Modeling

A Semantic Coverage Group (SCG) g is defined as a unique combination of class, descriptor, and subgroup attributes:

$$g = (\text{class} = c, \text{descriptor} = d, \text{subgroup} = s).$$

Class-level (e.g., majority vs. minority class) imbalance alone cannot capture the hidden skew in semantic concepts that appear within the same class. Descriptors such as visual semantic concepts (e.g., texture, geometric shape, color patterns, or lesion patterns: blue-white veil, pigmented network) represent interpretable, fine-grained semantics that models rely on for visual reasoning. Including descriptors in SCGs enables measuring imbalance at the semantic level, not just the class level; detecting underrepresented semantic patterns (rare descriptors); quantifying coverage-performance misalignment; and analyzing bias across semantic concepts. Therefore, SCGs demonstrate hidden structure in the data that would otherwise be invisible to class-only or subgroup-only analysis.

Coverage Calculation. For each SCG $g = (c, d, s)$, the training coverage c_g measures how often descriptor d occurs for class c within subgroup s . Let

$$\mathcal{D}_{c,s} = \{i : \text{class}_i = c, \text{subgroup}_i = s\},$$

denote the set of corresponding samples belonging to class c and subgroup s , and let $p_{i,d}$ be the descriptor probability for descriptor d on sample i . The *soft coverage* (expected

descriptor presence) is defined as

$$c_g = \frac{1}{|\mathcal{D}_{c,s}|} \sum_{i \in \mathcal{D}_{c,s}} p_{i,d},$$

providing a continuous estimate of descriptor prevalence under weak or noisy supervision (e.g., MONET probabilities). When descriptor probabilities need to be binarized or when descriptor annotations are already categorical, we compute *hard coverage* using a descriptor-specific threshold τ_d (e.g., categorical or clinician-verified):

$$c_g^\tau = \frac{1}{|\mathcal{D}_{c,s}|} \sum_{i \in \mathcal{D}_{c,s}} \mathbf{1}[p_{i,d} \geq \tau_d].$$

In this study, we focus on using *soft coverage* c_g for Semantic Coverage Imbalance (SCI) and Coverage Disparity Index (CDI) analysis.

Semantic Coverage Map. We visualize SCI (Fig. 5) using SCGs coverage heatmap and long-tailed distribution of coverage values. For SCG coverage heatmap, a matrix showing coverage c_g across classes \times descriptors \times subgroups showing sparse, underrepresented semantic intersections. We also visualize the ranked distribution of c_g to show the long-tailed imbalance in descriptor frequencies across SCGs. These visualizations show that SCI is widespread across both class-balanced (ISIC-DICM-17K = 1:1) and class-imbalanced (MILK10k \approx 1:10) datasets, motivating the semantic coverage-aware fairness learning.

Both datasets demonstrate that the SCG coverage heatmaps (Figs. 5a and 5c) show significant sparsity and an uneven representation of descriptors across each class-subgroup combination. In the MILK10k dataset, this imbalance is particularly pronounced, with many (minority class samples) SCGs showing almost no presence of descriptors (Fig. 5a). Meanwhile, the ISIC-DICM-17k dataset, although class-balanced, still shows significant divergence across descriptors and anatomical subgroups (Fig. 5c). The corresponding long-tail distributions (Figs. 5b and 5d) further illustrate that most SCGs fall within the extreme low-coverage range in both datasets, indicating that the issue of SCI persists regardless of class balance. This consistent long-tailed pattern underscores the need for SemCovNet, a Semantic Coverage-Aware Network that specifically addresses disparities in semantic and subgroup-level coverage.

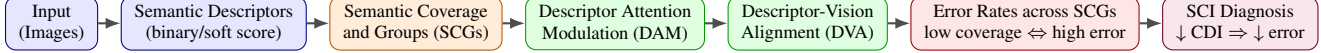


Figure 4. Conceptual workflow (grouping→coverage estimation→modulation→error analysis→diagnosis) of SemCovNet for addressing SCI.

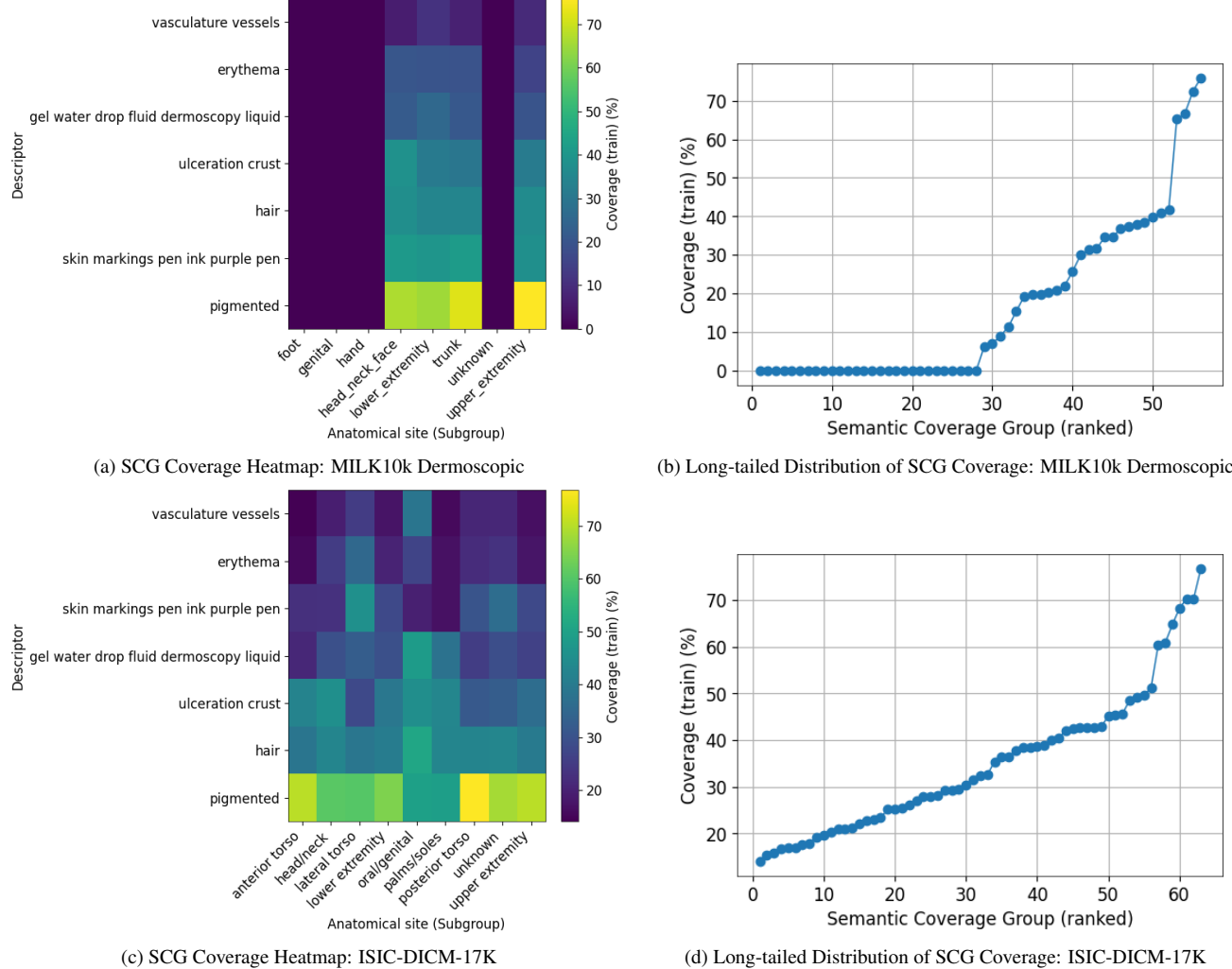


Figure 5. Semantic Coverage Imbalance (SCI) across SCGs for the melanoma class (MEL) on MILK10k ($\approx 1:10$ class-imbalanced) and ISIC-DICM-17K (1:1 class-balanced). (Left) The SCG Coverage Heatmap displays rows that correspond to semantic descriptors and columns that indicate demographic or contextual subgroups. The patterns observed are sparse and heterogeneous, showing significant variation in the presence of descriptors across different SCGs. (Right) Long-tailed distribution of SCG coverage values. Most SCGs exhibit low coverage, indicating severe semantic under-representation and highlights the long-tailed structure of SCI within the training data.

8. Coverage–Performance Disparity Analysis: Extended Interpretation

SCI occurs when SCGs with low coverage consistently have higher error rates. To quantify this effect, we use the CDI, which measures the alignment between training coverage and test-time error across different SCGs. For each SCG

g , we compute soft coverage $c_g \in [0, 1]$ using descriptor probabilities, and the group-wise error $e_g = 1 - \text{TPR}_g$. The CDI_g is the absolute Pearson correlation $\rho(\cdot)$ between coverage and error:

$$\text{CDI}_g = |\rho(c_g, e_g)|.$$

CDI Interpretation. If most low-coverage SCGs show

Table 7. Performance on CelebA (curated subset 1:5 class imbalance). We evaluate *Smiling* classification using 7 binary facial descriptors and *Male* as a subgroup. SCI appears in natural image datasets and semantic coverage-aware fairness learning generalizes to both soft- and hard-label concepts. AUROC (AUC), PR-AUC (PRA), Sens. @ 95% Spec (S@95), Balanced Accuracy (BAcc), Macro-F1 (M-F1), and Expected Calibration Error (ECE). Results are reported at the best epoch. SemCovNet performs competitively on CelebA’s hard labels, achieving the best PRA, BAcc, and M-F1, and the lowest CDI across models. The best results are in bold. Δ computed w.r.t. the best baseline and highlighted in bold.

Model	AUC↑	PRA↑	S@95↑	BAcc↑	M-F1↑	ECE↓	CDI↓ (Δ)	TPR _w ↑	TPR _{std} ↓
ENet-B0+CBL	0.9588	0.8777	0.8590	0.7423	0.8001	0.0205	0.3000	0.0000	0.3220
ENet-B0+ASL	0.8550	0.6527	0.5000	0.7375	0.7596	0.0366	0.6919	0.0000	0.2801
GroupDRO	0.9429	0.8876	0.8205	0.8625	0.7875	0.0315	0.2966	0.0000	0.2981
CLIP	0.9389	0.8119	0.7949	0.7861	0.8165	0.0415	0.3480	0.0000	0.3086
MONET	0.9361	0.8269	0.7308	0.5000	0.4551	0.1502	0.2828	0.0000	0.3059
SemCovNet (ours)	0.9682	0.9231	0.8333	0.8963	0.9025	0.0320	0.2737(- 0.01)	0.0000	0.3010

Table 8. Subgroup fairness comparison on MILK10K (Dermoscopic). We report CDI(\downarrow), TPR_w(\uparrow), TPR_{std}(\downarrow) across three subgroups, comparing the fairness-aware GroupDRO baseline with SemCovNet. *For each subgroup, we report the baseline fairness metric (left) and SemCovNet fairness metric (right). A \rightarrow B denotes the shift from the baseline to our model.* SemCovNet consistently reduces coverage–error correlation and improves robustness across Skin Tone, and Age, demonstrating fairness generalization beyond the Anatomic Site settings evaluated in the main paper.

Subgroup	CDI \downarrow	TPR _w \uparrow	TPR _{std} \downarrow
Site	0.4661 \rightarrow 0.0616	0.4167 \rightarrow 0.2667	0.1490 \rightarrow 0.2601
Skin tone	0.3330 \rightarrow 0.0226	0.3333 \rightarrow 0.5000	0.1522 \rightarrow 0.1386
Age	0.4085 \rightarrow 0.2560	0.0000 \rightarrow 0.0000	0.3241 \rightarrow 0.3187

poor recall (low TPR) while high-coverage SCGs perform well \rightarrow CDI is high, indicating severe SCI. Therefore, if SemCovNet reduces the slope in the coverage–error performance across SCGs \rightarrow CDI drops, indicating improved semantic fairness. In this study, we calculate CDI across all SCGs to evaluate how closely the model’s performance correlates with descriptor coverage across all combinations of semantic concepts, classes, and subgroups. Therefore, we deliberately consider our interpretation of the CDI to the low-coverage scenario, which captures the core failure mode of SCI and maintains the validity of CDI as a semantic fairness measure.

9. Generalization to Non-Medical Domains: Performance on CelebA

To verify that the SCI occurs naturally beyond medical imaging, we evaluated SemCovNet on the CelebA¹ facial attribute dataset using a curated subset of 5,000 samples from a 1:5 class-imbalanced *Smiling* classification task. We

¹<https://huggingface.co/datasets/flwrlabs/celeba>

selected 7 binary attributes *Heavy Makeup*, *Bangs*, *Eye-glasses*, *Mustache*, *Black Hair*, *Pale Skin*, and *High Cheekbones* and included *Male* as a subgroup to create SCGs. Although CelebA provides hard binary attribute labels, rather than the continuous soft descriptors for which SemCovNet is designed, SCI still exists in the form of latent, weak, and co-occurring concept imbalance. This experiment allows us to evaluate whether SemCovNet’s semantic fairness principles generalize to natural images with binary concept supervision.

SemCovNet is optimized for continuous descriptor probabilities, which may lead to slight performance differences when applied to the noisier hard labels of CelebA. However, SemCovNet maintains strong representation quality while also improving fairness measures. Table 7 results show that SemCovNet achieves the best PR-AUC, Balanced Accuracy, Macro-F1 score, and the lowest CDI, indicating reduced coverage–error misalignment across SCGs. Although the TPR_w reaches zero due to the extreme sparsity of certain SCGs, SemCovNet still maintains competitive TPR_{std} variance compared to baseline models. These analyses highlight the presence of SCI in natural vision datasets and show that semantic coverage–aware learning (SemCovNet) remains effective even when concept labels are binary, showing robustness across soft- and hard-label settings.

10. Fairness Evaluation across Sensitive Subgroup

We study cross-attribute fairness, which asks: *Does fairness generalize to other protected or sensitive attributes in the SCI condition?* To answer this, we extend our fairness evaluation beyond the anatomical-site subgroups analyzed in the main paper, incorporating *Skin Tone* and *Age* from the MILK10k Dermoscopic dataset. We compare against GroupDRO, which we consider the fairness-aware baseline and also the strongest overall baseline model in this study.

Table 9. Cross-domain semantic alignment on MILK10K. Align-cos and R@1 measure descriptor–vision alignment in dermoscopic and clinical domains. $\Delta\text{Align-gap} = |\text{Align-cos}(\text{Dermoscopic}) - \text{Align-cos}(\text{Clinical})|$. DVA enhances alignment in both domains. $\Delta\text{Align-gap} \downarrow$ indicates a stable and consistent semantic grounding across different domains.

Method	Dermoscopic		Clinical		$\Delta\text{Align-gap} \downarrow$
	Align-cos \uparrow	R@1 \uparrow	Align-cos \uparrow	R@1 \uparrow	
Visual-only	-0.0372	0.0325	-0.0630	0.0306	0.026
SDM	0.0229	0.0074	0.0138	0.0232	0.009
SDM+DVA (Ours)	0.7862	0.8401	0.5581	0.2990	0.228

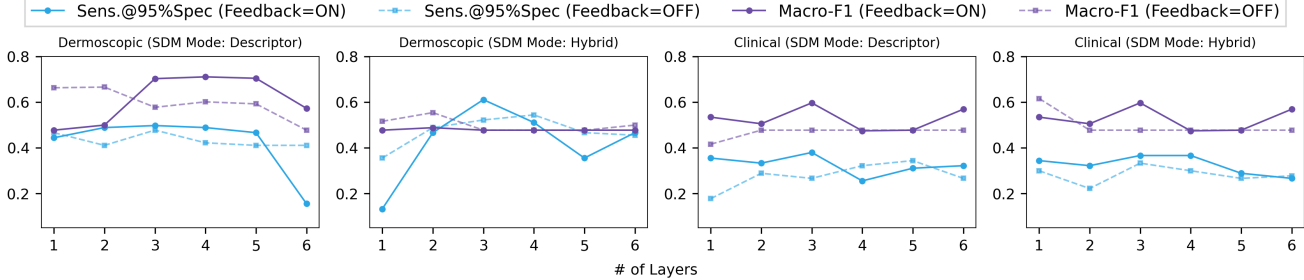


Figure 6. Ablation on Semantic Encoder depth. Effect of the number of layers used for descriptor feedback (token \rightarrow descriptor refinement) on MILK10k Dermoscopic (left) and Clinical (right) datasets. Each subplot compares performance with feedback ON (solid) vs. OFF (dashed) across 6 layers. Feedback consistently refines descriptor representations in deeper stages, with the 3rd layer achieving the best overall performance–depth trade-off.

Table 8 results show that across all subgroup types, SemCovNet consistently lowers CDI relative to the baseline, reducing coverage–error misalignment. SemCovNet also improves TPR_w for *Skin tone* while maintaining competitive TPR variance. These results demonstrate that SemCovNet’s fairness generalizes across protected and sensitive attribute families, extending beyond anatomical site to include demographic attributes such as skin tone and age.

11. Cross-Modality Semantics

SemCovNet learns domain-invariant semantics for descriptors. To validate its effectiveness, we measure how well descriptor–vision alignment is preserved across domains by computing it separately on dermoscopic and clinical datasets of MILK10k. We measure cosine similarity (Align-cos) between descriptors and visual embeddings, retrieval accuracy (R@1) for matching descriptor–image pairs, and a cross-domain stability metric $\Delta\text{Align-gap}$, which represents the absolute difference between the dermoscopic and clinical Align-cos values.

In Table 9, the visual-only approach shows nearly zero (and even negative) alignment in both domains, demonstrating a lack of meaningful semantic grounding. While SDM weakens alignment, it maintains consistency across domains. In contrast, SDM combined with DVA improves alignment in both dermoscopic (0.786) and clinical (0.558) settings, effectively recovering strong semantic descriptors

across different acquisition domains. The $\Delta\text{Align-gap}$ remains small relative to the alignment magnitude, indicating that DVA learns a shared descriptor–vision space that transfers across domain shifts.

12. Additional Ablation Study: Depth of Semantic Encoder

We analyze how the depth of the network and the feedback from descriptors to features affect the semantic refinement within the Semantic Encoder. Specifically, we implement a feedback connection, which updates descriptor tokens from one layer back into the descriptor projection. This allows later layers to refine descriptor embeddings using features computed in earlier layers. To evaluate the effects of these feedback connections, we varied from 1 to 6 layers and toggled feedback connections (token \rightarrow descriptor) across layers to refine descriptor representations in subsequent layers through descriptor–feature feedback. If feedback is ON, refine the descriptor via token \rightarrow descriptor and rebuild the SDM. Increasing depth enhances semantic refinement, while feedback stabilizes earlier representations. Figure 6 presents both MILK10k Dermoscopic and Clinical results, showing that descriptor feedback consistently enhances sensitivity and Macro-F1 performance across depths. However, performance saturates beyond three layers, indicating diminishing returns from additional depth. The three layer configuration with

feedback achieves the best balance between fairness and reliability.